

**Nonholonomic diffusion of a stochastic sled**Peter Jung,<sup>1</sup> Giampiero Marchegiani,<sup>2</sup> and Fabio Marchesoni<sup>2,3</sup><sup>1</sup>*Department of Physics and Astronomy, and Quantitative Biology Institute, Ohio University, Athens, Ohio 45701, USA*<sup>2</sup>*Dipartimento di Fisica, Università di Camerino, I-62032 Camerino, Italy*<sup>3</sup>*Center for Phononics and Thermal Energy Science, Tongji University, Shanghai 200092, People's Republic of China*

(Received 3 March 2015; revised manuscript received 10 October 2015; published 13 January 2016)

A sled is a stylized mechanical model of a system which is constrained to move in space in a specific orientation, i.e., in the direction of the runners of the sled or a blade. The negation of motion transverse to the runners renders the sled a nonholonomic mechanical system. In this paper we report on the unexpected and fascinating richness of the dynamics of such a sled if it is subject to random forces. Specifically we show that the ensuing random dynamics is characterized by relatively smooth sections of motion interspersed by episodes of persistent tumbling (change of orientation) and sharp reversals resembling the random walks of bacterial cells. In the presence of self-propulsion, the diffusivity of the sled can be enhanced and suppressed depending on the directionality and strength of the propulsive force.

DOI: [10.1103/PhysRevE.93.012606](https://doi.org/10.1103/PhysRevE.93.012606)**I. INTRODUCTION**

Constraints are of key importance for many mechanical systems and determine their dynamic behavior. For example, a mathematical pendulum is constrained by the distance of the pivot and the bob, and this constraint, in conjunction with gravity, determines its oscillatory, rotational, and—in the presence of a driving force—chaotic dynamics. Holonomic constraints limit the movement of the system to a subspace and correspondingly reduce the degrees of freedom and numbers of variables necessary to describe the system. Nonholonomic constraints limit the movement of the system only locally while allowing the system to fully explore its state space. A simple model for a nonholonomic system which captures all relevant features, but yet can be solved analytically, is the Chaplygin-Carathéodory (CC) sled [1–7]. Such a sled can move anywhere in a two-dimensional (2D) plane, but the direction of its velocity is locally constrained by the orientation of a blade which can rotate around a pivot point. Each point in the 2D plane can be reached, but prohibition of sideways motion renders motion planning necessary. Most automotorists experience such dynamics (some with more frustration than others) and the need for motion planning, when forced to execute the process of “parallel parking” or when trying to maneuver a vehicle with a trailer backward into a garage [8].

The dynamics of such a system is remarkably rich as the nonholonomic constraint couples orientational and translational motion of the sled. This leads to translational instabilities that depend on the orientation of the sled with respect to the direction of motion, establishing stable and unstable orientations of motion. The main focus of this paper is on the stochastic behavior of a microscopic sled, subject to fluctuating forces of the environment, a prototype of nonholonomic Brownian motion. While one expects diffusive behavior of such a sled, it is clear that due to the local constraints of motion and the coupling of orientation and translation, the diffusive behavior is far richer than that of traditional Brownian particles. It is demonstrated, for example, that the random motion of the sled is interspersed by bursts of tumbling.

As the literature on the dynamics of such systems is scattered over time and journals (much of it not available in the

English language), we start off this paper with a brief summary of the nonlinear dynamics of the deterministic 2D CC sled, which might help the reader better appreciate the differences and similarities with our model of the stochastic sled. In Sec. III we investigate the dynamics of a 2D stochastic sled coupled to an equilibrium heat-bath. While the Brownian motion of the sled is nonstationary, its dynamics in momentum space (velocity and angular velocity) is stationary, and we establish average velocities, angular velocities, and the partition of translational and rotational energies. As expected the sled exhibits diffusive behavior over longer time scales, but the diffusivity depends on the coupling between translation and orientation. The diffusive behavior is particularly interesting in the presence of a propulsion force (see Sec. IV). The diffusivity can be amplified if the sled is driven along its stable direction or it can be strongly suppressed when it is propelled along its unstable direction. The latter results in a rotational bistability, where the sled switches between clockwise and counterclockwise rotation. Analytical predictions obtained through an approximated linearization scheme are shown to compare well with the outcome of numerical simulations.

Finally, in Sec. V we comment on the observed similarities between the diffusive dynamics of a stochastic self-propelled sled and active microswimmers, although we don't suggest that the stochastic sled model is a bona-fide model for microswimmers [9–11].

**II. THE CHAPLYGIN-CARATHÉODORY SLED**

In the absence of external drives, the sled's equations of motion were derived by Chaplygin, within the Lagrangian formalism [1], and by Carathéodory, through a force balance method [2],

$$\begin{aligned} m\dot{v} &= ma\omega^2, \\ I_P\dot{\omega} &= -mav, \end{aligned} \quad (1)$$

where  $v$  and  $\omega$  are, respectively, the linear velocity along the oriented sled axis  $\hat{x}'$  and the angular velocity around the pivot point. For simplicity, the center of mass  $O$  and the pivot point  $P$  are assumed to rest on the sled's axis at a distance

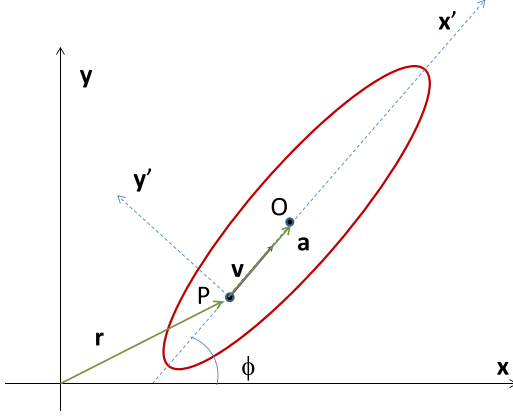


FIG. 1. Sketch of an ellipsoidal CC sled. The pivot point  $P$  and the center of mass  $O$  sit on the major sled axis; the inertial reference frame  $x, y$  and the body reference frame  $x', y'$  are introduced in the text.

$a$  that quantifies the eccentricity of the constraint (Fig. 1). The velocity coordinates  $v$  and  $\omega$  are related to the spatial coordinates of the sled's pivot point  $P$  in the plane,  $x$  and  $y$ , and to its orientation,  $\phi$ , by the equations

$$\dot{x} = v \cos \phi, \quad \dot{y} = v \sin \phi, \quad \dot{\phi} = \omega, \quad (2)$$

where  $\phi$  denotes the angle between the sled and the positive  $x$  axis.

For practical purposes we make use of Steiner's identity,  $I_P = I_O + ma^2$ , to relate the sled's moments of inertia relative to  $P$ ,  $I_P$ , and the center of mass,  $I_O$ , and then scale all lengths by means of the characteristic length  $l$ , defined by  $I_O \equiv ml^2$ ; that is,  $x \rightarrow x/l$ ,  $y \rightarrow y/l$ ,  $v \rightarrow v/l$ ,  $a \rightarrow \alpha = a/l$ , and  $I_P = 1 + \alpha^2$ . The CC equations can thus be reformulated as

$$\begin{aligned} \dot{v} &= \alpha \omega^2, \\ \dot{\omega} &= -\frac{\alpha}{1 + \alpha^2} \omega v. \end{aligned} \quad (3)$$

In the following we treat  $\alpha$  as a tunable parameter with  $\alpha \in [0, \infty]$ . However, one should not forget that for a homogeneous 2D body of given mass, the distance  $OP$  is no larger than half the maximum diameter; that is,  $\alpha \leq \alpha_l$ , where  $\alpha_l$  depends on the particle conformation. For instance, for a thin rod,  $\alpha_l = \sqrt{3}$ , and for a solid disk,  $\alpha_l = 2$ .

Without entering the details of the derivation of CC Eqs. (3), we limit ourselves to a qualitative interpretation of the sled dynamics in the ‘‘momentum’’ space,  $v$  and  $\omega$ . Due to the constraint, the longitudinal axis of the sled and its velocity  $v$  is always tangential to the  $P$  trajectory. The first Eq. (3) simply tells us that the sled accelerates along its long axis with the centrifugal acceleration,  $\alpha \omega^2$ , generated by its simultaneous rotation around  $P$ . The second equation equals the time derivative of the sled's angular momentum relative to the pivot point, to the torque associated with the tangential force applied in  $P$ .

On a first glance it may appear that such a model is only narrowly defined through the nonholonomic constraint. Carathéodory himself first raised the question of whether an unconstrained dissipative system with a very large damping

constant for motion perpendicular to the long axis can be modeled as a nonholonomic constrained one. Carathéodory himself ruled out this option [2], Fufaev [6], however, proved rigorously the contrary. Today we know that a large class of nonholonomic constraints is obtainable by means of appropriate procedures involving some ‘‘infinite’’ friction limit of an appropriate Hamiltonian system [3].

The nonlinear Eqs. (3) are explicitly integrable [3]. To this purpose we first notice that the sled's kinetic energy is a constant of motion. On multiplying the CC equations, respectively, by  $v$  and  $\omega$  and then adding them up term by term we obtain  $d[v^2 + (1 + \alpha^2)\omega^2]/dt = 0$ , which implies that the kinetic energy,

$$E = \frac{1}{2}[v^2 + (1 + \alpha^2)\omega^2], \quad (4)$$

is conserved. This result is consistent with the fact that the constraint forces, holonomic or not, do not do work either parallel or perpendicular to the sled's axis [12]. Note that the translational and rotational degrees of freedom are coupled by the constraint in  $P$  so that the relevant kinetic energy terms are not separately conserved.

The sled's equations, Eqs. (3), can be solved analytically in the 2D momentum space  $v, \omega$ , namely, for a given value of  $E$  and  $v(0) = 0$ ,

$$v(t) = v_E \tanh\left(\frac{\alpha}{1 + \alpha^2} v_E t\right) \quad (5)$$

$$\omega(t) = \pm \frac{v_E / \sqrt{1 + \alpha^2}}{\cosh[\alpha v_E t / (1 + \alpha^2)]}, \quad (6)$$

with  $v_E = \sqrt{2E}$ . The sled's orbits in the momentum plane are elliptical arcs of Eq. (4). However, the pivot point  $P$  does not trace an entire ellipse, because the positive  $v$  axis attracts all solutions. Indeed, on each ellipse there exists one attracting orbital point representing the asymptotic solution,  $(v, \omega) = (v_E, 0)$ , and two equivalent unstable tumbling points,  $(0, \pm \sqrt{2E})$ .

The  $P$  trajectories in the  $x, y$  plane can be determined by integrating Eqs. (2) for the known solutions  $v(t)$  and  $\omega(t)$ . The analytical expression of  $\phi(t)$  is easily obtained by inserting Eq. (6) into the third Eq. (2) and integrating with respect to time for  $\phi(0) = 0$ ; that is,

$$\phi(t) = \pm \frac{\sqrt{1 + \alpha^2}}{\alpha} \arctan\left[\sinh\left(\frac{\alpha}{1 + \alpha^2} v_E t\right)\right]. \quad (7)$$

Equations (2) for  $x(t)$  and  $y(t)$  can be solved numerically only, except for a few particular cases [1,7]. As illustrated in Fig. 2, a sled is launched at  $t = -\infty$  at an infinite distance with a negative velocity,  $-v_E$ , and zero angular velocity. A negative velocity implies that the sled is moving with a negative orientation with respect to its internal coordinate axis  $\hat{x}'$  (see Fig. 1), i.e., pivot point,  $P$ , ahead of center of mass,  $O$ . In this situation, the sled decelerates with time since the first Eq. (3) implies  $\dot{v} > 0$  and the rate of rotation increases, thereby preserving its total energy  $v_E^2/2$ . Hence, the negative orientation of motion constitutes the unstable orientation of motion mentioned earlier. At  $t = 0$  the sled reaches zero velocity at a maximum turning rate  $\omega$  but subsequently continues to move with a positive velocity in a positive  $x$

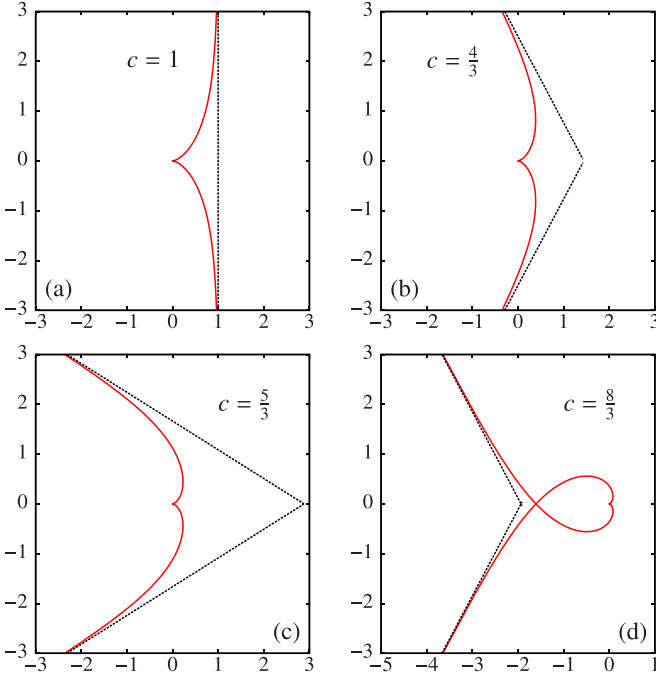


FIG. 2. Examples of deterministic CC trajectories for different  $\Delta\phi_\infty = \pi c$ , with  $c = \sqrt{(1 + \alpha^2)}/\alpha^2$ .

direction. A positive  $v$  indicates that the sled is now moving in the positive direction with respect to its axes  $\hat{x}'$ , i.e., center of mass ahead of the pivot point. The second Eq. (3) now implies that the rate of rotation is decreasing while the first equation implies that the sled will accelerate until it reaches its asymptotic velocity  $v_E$  at  $t = \infty$ . During this phase of the motion, the sled moves in its stable orientation. We have termed this sequence of events which results in an abrupt change of velocity (see below) and a change in orientation a “tumble,” inspired by the tumbling of self-propelled *Escherichia coli* bacterial cells. The sled’s incoming and outgoing directions,  $\phi_{\pm\infty} = \pm\pi\sqrt{1 + \alpha^2}/2\alpha$ , are mirror symmetric with respect to the tumbling axis,  $\phi = 0$ , and the angle between them is given by  $\Delta\phi_\infty = \pi\sqrt{1 + \alpha^2}/\alpha$ . Under the condition  $\Delta\phi_\infty = n\pi$ , with  $n$  being a positive integer, the incoming and the outgoing directions are parallel;  $n - 1$  is the number of *full* turns executed by the sled in addition to the tumbling event at  $t = 0$ .

### III. THE STOCHASTIC SLED

A miniaturized CC sled placed in a fluctuating environment in equilibrium at temperature  $T$  will be subject to viscous and random perturbations, which must be incorporated in Eqs. (3), namely,

$$\begin{aligned} \dot{v} &= \alpha\omega^2 - \gamma v + \sqrt{\gamma\theta}\xi_v(t), \\ \dot{\omega} &= -\frac{\alpha}{1 + \alpha^2}\omega v - \Gamma\omega + \sqrt{\frac{\Gamma\theta}{1 + \alpha^2}}\xi_\omega(t), \end{aligned} \quad (8)$$

where  $\xi_v(t)$  and  $\xi_\omega(t)$  are stationary Gaussian noises with zero mean and autocorrelation functions  $\langle \xi_i(t)\xi_j(0) \rangle = 2\delta_{ij}\delta(t)$ , with  $i, j = v, \omega$  and  $\theta = kT/l^2$ . The noise force  $\xi_v(t)$  accelerates the sled along its long axis, while  $\xi_\omega(t)$  acts like a stochastic torque driving the rotation of the sled around its

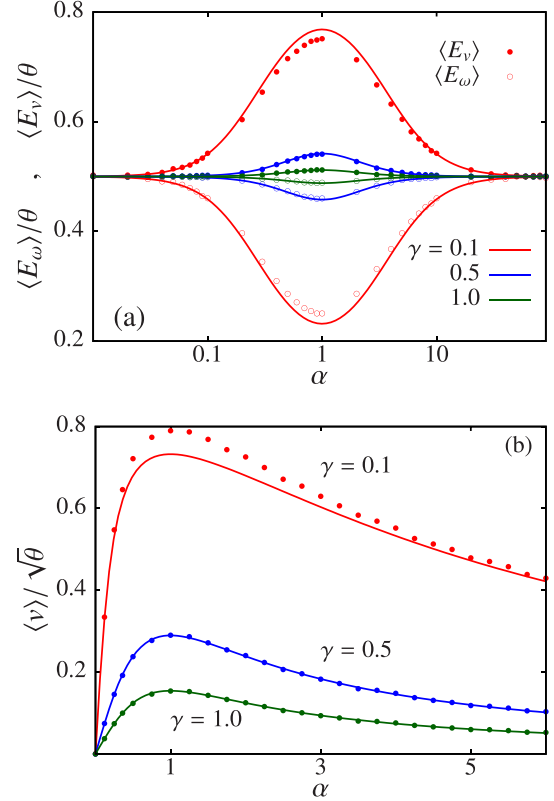


FIG. 3. Stochastic CC sled with  $p = 0$ : (a)  $\langle E_v(\alpha) \rangle$  and (b)  $\langle v(\alpha) \rangle$  vs  $\alpha$  for  $\theta = 0.1$  and different values of  $\gamma = \Gamma$ . Symbols represent the data points obtained by numerically integrating Eqs. (8); the solid curves are the analytical approximations for  $\epsilon \ll 1$  derived in the text, Eqs. (15) and (17).

pivot point,  $P$ . We treat the damping constants  $\gamma$  and  $\Gamma$  for translation and rotation, respectively, as independent model parameters, although in thermal equilibrium they are known to be related [9].

Coupling the CC sled to a fluctuating environment stabilizes its trajectories in the momentum space  $v, \omega$ . The ensuing stationary stochastic dynamics can be characterized in terms of the first two moments of the variables  $v$  and  $\omega$ , that is, by computing the average velocity  $\langle v \rangle$  and the average translational,  $\langle E_v(\alpha) \rangle = \langle v^2 \rangle / 2$ , and rotational kinetic energy,  $\langle E_\omega(\alpha) \rangle = (1 + \alpha^2)\langle \omega^2 \rangle / 2$  (Fig. 3). In the overdamped regime, i.e., for large  $\gamma$  and  $\Gamma$ , such quantities can be evaluated analytically.

#### A. Average total kinetic energy

If the CC sled is coupled to the heat bath symmetrically with  $\Gamma = \gamma$ , its energy can be proven to satisfy the equipartition energy. On multiplying Eqs. (8), respectively, by  $v$  and  $\omega$ , one derives two simple coupled multiplicative stochastic equations for the translational part,  $E_v = v^2/2$ , and the rotational part,  $E_\omega = (1 + \alpha^2)\omega^2/2$ , of the system kinetic energy:

$$\begin{aligned} \dot{E}_v &= \alpha\omega^2 v - 2\gamma E_v + \sqrt{2\gamma\theta} E_v \xi_{E_v}(t), \\ \dot{E}_\omega &= -\alpha\omega^2 v - 2\gamma E_\omega + \sqrt{2\gamma\theta} E_\omega \xi_{E_\omega}(t), \end{aligned} \quad (9)$$

where  $\xi_{E_v}(t)$  and  $\xi_{E_\omega}(t)$  have the same properties as  $\xi_v(t)$  and  $\xi_\omega(t)$  in Eq. (8) and the multiplicative noise terms are defined

according to the Stratonovitch prescription [13]. According to Ito's prescription Eqs. (9) must be rewritten as

$$\begin{aligned}\dot{E}_v &= \alpha\omega^2 v - 2\gamma E_v + \gamma\theta + \sqrt{2\gamma\theta E_v} \xi_{E_v}(t), \\ \dot{E}_\omega &= -\alpha\omega^2 v - 2\gamma E_\omega + \gamma\theta + \sqrt{2\gamma\theta E_\omega} \xi_{E_\omega}(t).\end{aligned}\quad (10)$$

Adding these two equations term to term yields a simple Langevin equation for the total kinetic energy,  $E = E_v + E_\omega$ , which, transformed back into the more compact Stratonovich notation, reads

$$\dot{E} = -2\gamma E + \gamma\theta + \sqrt{2\gamma\theta E} \xi_E(t), \quad (11)$$

with  $\xi_E(t)$  defined, again, like the noises in Eq. (9). The explicit solution of this equation shows that the sled energy thermalizes independently of  $\alpha$  with  $\langle E(\alpha) \rangle = \theta$ ; the corresponding Fokker-Planck equation for the stochastic variable  $E$  returns a stationary probability density of Boltzmann's type,  $P(E) = e^{-E/\theta}$ .

We remark here that the thermalization law of Eq. (11) applies only for  $\gamma = \Gamma$ . Still this is a remarkable property when one considers that, due to the nonholonomic nature of the system at hand, the Langevin Eqs. (8) do not satisfy a detailed balance [14]. As a matter of fact, for  $\alpha \neq 0$ , the stationary solution of the corresponding 2D Fokker-Planck equation in the momentum space  $v, \omega$  is not of the Boltzmann type.

### B. Velocity moments

The stochastic average of the first Eq. (8) yields the exact identities

$$\langle v \rangle = \alpha \langle \omega^2 \rangle / \gamma, \quad \langle \omega \rangle = 0. \quad (12)$$

The first equation immediately tells us that the average velocity  $\langle v \rangle$  only vanishes for  $\alpha = 0$ , i.e., when the sled rotates around its center of mass. This means that in the average the sled spends the same time moving in positive and negative orientation. For positive  $\alpha$ , the average velocity  $\langle v \rangle$  is positive, indicating that the sled preferably moves in a positive direction. This is the consequence of the instability of the movement in the negative orientation we described in the previous section. This bias towards a certain orientation of the sled during movement does not imply a bias in any spatial direction of the movement of the sled.

The first identity of Eq. (12) can be used to linearize the CC equations as

$$\begin{aligned}\dot{v} &= \gamma \langle v \rangle - \gamma v + \sqrt{\gamma\theta} \xi_v(t), \\ \dot{\omega} &= -\frac{\alpha^2}{1+\alpha^2} \frac{\langle \omega^2 \rangle}{\gamma} \omega - \Gamma \omega + \sqrt{\frac{\Gamma\theta}{1+\alpha^2}} \xi_\omega(t).\end{aligned}\quad (13)$$

Such a linearization procedure holds good for

$$\epsilon = \sqrt{\theta/\gamma\Gamma} [\alpha/(1+\alpha^2)] \ll \sqrt{\Gamma/\gamma}.$$

Indeed, the error made on replacing  $v$  by  $\langle v \rangle$  in the second Eq. (8) is of the order of  $\sqrt{\theta\omega\alpha}/(1+\alpha^2)$ , which we want to be small relative to the modulus of the damping term,  $-\Gamma\omega$ , we kept in the linearized Eq. (13) [Fig. 3(b)].

Accordingly, the results below apply for any  $\alpha$  in the overdamped regime,  $\theta/\Gamma^2 \ll 1$ , and for any thermal length,  $\theta/\gamma\Gamma$ , in the limits  $\alpha \rightarrow 0$  and  $\alpha \rightarrow \infty$ . Multiplying both

sides of the second equation by  $\omega$  and taking the stochastic average yields the moment equation

$$\frac{1}{2} \frac{d}{dt} \langle \omega^2 \rangle = -\Gamma \langle \omega^2 \rangle - \frac{\alpha^2}{1+\alpha^2} \frac{\langle \omega^2 \rangle^2}{\gamma} + \frac{\Gamma\theta}{1+\alpha^2} = 0,$$

whence, solving for  $\langle \omega^2 \rangle$  in steady state,

$$\langle \omega^2(\epsilon) \rangle = 2\theta / [(1+\alpha^2)(\sqrt{1+4\epsilon^2} + 1)]. \quad (14)$$

Within the limits of validity of our linearization procedure, the following approximations apply [Fig. 3(a)]:

$$\langle E_\omega(\alpha) \rangle = (1+\alpha^2) \langle \omega^2(\epsilon) \rangle / 2 = \theta / (\sqrt{1+4\epsilon^2} + 1), \quad (15)$$

$$\langle v(\alpha) \rangle = \alpha \langle \omega^2(\epsilon) \rangle / \gamma, \quad (16)$$

and

$$\langle E_v(\alpha) \rangle = [\langle v(\alpha) \rangle^2 + \theta] / 2 = [(\alpha \langle \omega^2(\epsilon) \rangle / \gamma)^2 + \theta] / 2. \quad (17)$$

The average energy  $E_v$  increases with increasing eccentricity  $\alpha$  because the phases of movement where the sled moves in its stable orientation increase in duration, reducing the tumbling events and hence the rotational energy  $E_\omega$ . Note that for  $\gamma = \Gamma$  the approximate expressions in Eqs. (15) and (17) satisfy the exact identity  $\langle E(\alpha) \rangle_v + \langle E(\alpha) \rangle_\omega = \theta$ , up to terms of order  $\epsilon^2$ .

### C. Diffusion coefficient

The *spatial* diffusion of the stochastic CC sled in the plane  $x, y$  is governed by the asymptotic diffusion law:

$$\lim_{t \rightarrow \infty} \langle \mathbf{r}^2(t) \rangle = 4Dt.$$

$D$  can be calculated from Eqs. (2) and (8) by applying Kubo's formula [15],

$$D = \int_0^\infty C(t) dt, \quad (18)$$

where  $C(t) = \langle v(t) \cos \phi(t) v(0) \cos \phi(0) \rangle$ . For finite values of  $\alpha$  the diffusion constant  $D$  can be estimated as follows.

(i) We assume that  $C(t)$  factorizes as  $C(t) \simeq \langle v(t)v(0) \rangle \langle \cos \phi(t) \cos \phi(0) \rangle$ . This assumption is consistent with the linearization procedure introduced in Sec. III C and applies for  $\epsilon \ll 1$ .

(ii) On combining the third Eq. (2) and the second Eq. (13), we calculate the *orientational* diffusion law following [14]

$$\langle \cos \phi(t) \cos \phi(0) \rangle = (1/2) \exp[-\langle \phi^2(t) \rangle / 2],$$

with

$$\langle \phi^2(t) \rangle = 2[\theta\Gamma/\tilde{\Gamma}^2(1+\alpha^2)][t - (1 - e^{-\tilde{\Gamma}t})/\tilde{\Gamma}] \quad (19)$$

and  $\tilde{\Gamma} = \Gamma[1 + \alpha^2/(1 + \alpha^2) \langle \omega^2(\epsilon) \rangle / (\gamma\Gamma)]$ . For  $\epsilon \ll 1$  one sees immediately that  $\tilde{\Gamma} \simeq \Gamma(1 + \epsilon^2)$ , so that  $\tilde{\Gamma}$  can be conveniently replaced by  $\Gamma$ . Accordingly,  $\lim_{t \rightarrow \infty} \langle \phi^2(t) \rangle = 2D_\phi t$ , where

$$D_\phi = \theta / [\Gamma(1 + \alpha^2)] = \epsilon^2 \gamma (1 + \alpha^2) / \alpha^2 \quad (20)$$

is the sled's angular diffusion constant in leading order of  $\epsilon$ .

(iii) From the linearized Langevin equation for  $v$  in Eq. (13) we obtain immediately the autocorrelation function of the longitudinal velocity:

$$\langle v(t)v(0) \rangle \simeq \langle v \rangle^2 + \theta e^{-\gamma t}.$$

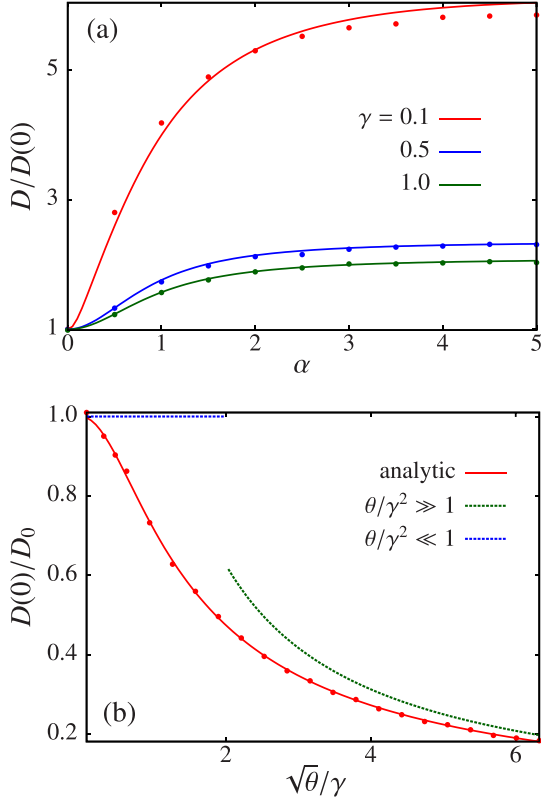


FIG. 4. Diffusion of the stochastic CC sled with  $p = 0$ . (a)  $D(\alpha)$  vs  $\alpha$  for  $\theta = 0.1$  and different values of  $\gamma = \Gamma$ . Symbols represent the data points obtained by numerically integrating Eqs. (26); the solid curves have been obtained by integrating Kubo's formula, Eq. (21) with  $\langle \phi^2(t) \rangle$  given by Eq. (19). (b) Numerical data for  $D(0)/D_0$  with  $D_0 = \theta/2\gamma$  vs  $\theta$  compared with the predicted behaviors for small  $\theta$ , Eq. (24), and large  $\theta$ , Eq. (25) (dashed curves).

(iv) Thanks to the factorization in (i), Kubo's integral of Eq. (18) is finally approximated to

$$D = \frac{1}{2} \int_0^\infty (\langle v \rangle^2 + \theta e^{-\gamma t}) e^{-\langle \phi^2(t) \rangle / 2} dt, \quad (21)$$

with  $\langle v \rangle$  and  $\langle \phi^2(t) \rangle$  given, respectively, in Eqs. (16) and (19). A comparison between simulation data and predictions based on Kubo's formula is displayed in Fig. 4(a).

The integral in Eq. (21) can be carried out explicitly for appropriate parameter domains. For instance, in the limit  $D_\phi \ll \Gamma$ , i.e., for  $\epsilon^2 \ll \alpha^2 / (1 + \alpha^2) (\Gamma / \gamma)$  or, equivalently,  $\theta / \Gamma^2 \ll 1 + \alpha^2$ , the  $\cos \phi$  autocorrelation function decays fast enough to justify the approximation  $\langle \phi^2(t) \rangle = 2D_\phi t$  in the exponential function [see Eq. (19)]. In conclusion,

$$\begin{aligned} D(\alpha) &= \frac{\theta}{2(\gamma + D_\phi)} + \frac{\langle v(\alpha) \rangle^2}{2D_\phi} \\ &\simeq \frac{\theta}{2\gamma} \left[ 1 + \frac{\Gamma}{\gamma} \frac{\alpha^2}{1 + \alpha^2} \right], \end{aligned} \quad (22)$$

where the second identity holds for  $\epsilon \rightarrow 0$  and  $D_\phi \ll \gamma$ .

Moreover, for  $\alpha = 0$  the integration in Eq. (18) can be carried out exactly because the factorization of  $C(t)$  in (i) and the expression in Eq. (19) for  $\langle \phi^2(t) \rangle$  (with  $\tilde{\Gamma} = \Gamma$ ) are

rigorous. A straightforward calculation yields

$$D(0) = \frac{\theta}{2\Gamma} \Gamma(a) \sum_{k=0}^{\infty} \frac{b^k}{\Gamma(1+k+a)}, \quad (23)$$

with  $a = \gamma / \Gamma + \theta / \Gamma^2$ ,  $b = \theta / \Gamma^2$ , and  $\Gamma(x)$  denoting the gamma function.

The low- and high-temperature limits of  $D(0)$  can be either extracted from Eq. (23) or calculated from the approximate integral in Eq. (21). For both  $\theta / \Gamma^2 \ll 1$  and  $D_\phi \ll \gamma$ , this is the same as setting  $\alpha = 0$  in Eq. (22), i.e.,

$$D(0) = \frac{\theta}{2\gamma} \frac{1}{1 + \theta / \gamma \Gamma}. \quad (24)$$

In the high-temperature regime,  $\theta / \Gamma^2 \gg 1$  with  $D_\phi \ll \gamma$ , the autocorrelation function of  $\cos \phi$  decays much slower than that of  $v$ , so that in Eq. (21) it has to be approximated by  $\langle \phi^2(t) \rangle \simeq \theta t^2$ , and Kubo's formula yields

$$\begin{aligned} D(0) &= \sqrt{\pi \theta / 8} e^{\gamma^2 / 2\theta} \text{Erfc}(\gamma / \sqrt{2\theta}) \\ &\simeq \frac{1}{2} \sqrt{\frac{\pi \theta}{2}} \left[ 1 - \sqrt{\frac{2}{\pi}} \frac{\gamma}{\sqrt{\theta}} + \dots \right], \end{aligned} \quad (25)$$

where  $\text{Erfc}(x)$  denotes the complementary error function.

We have worked out this tedious algebra because the final result is of some physical interest. At high temperature the stochastic CC sled undergoes normal diffusion, but its diffusion coefficient is not of the Einstein's type;  $D(0)$  grows with the square root of the temperature and not linearly with it, like for a regular Brownian particle [16]. This conclusion can be easily generalized to sleds with any  $\alpha$ , as proven by direct integration of Eq. (21) and supported by numerical simulation (not shown).

#### IV. THE STOCHASTIC MOTORSLED

When equipped with an engine, the sled propels itself under the action of a force  $p$  parallel to its axis. The engine pushes the motorsled in the stable direction from  $P$  to  $O$  for  $p > 0$  and in the unstable direction from  $O$  to  $P$  for  $p < 0$ . This corresponds to adding a self-propulsion term in the Langevin Eqs. (8), which now read

$$\begin{aligned} \dot{v} &= \alpha \omega^2 - \gamma v + p + \sqrt{\gamma \theta} \xi_v(t), \\ \dot{\omega} &= -\frac{\alpha}{1 + \alpha^2} \omega v - \Gamma \omega + \sqrt{\frac{\Gamma \theta}{1 + \alpha^2}} \xi_\omega(t). \end{aligned} \quad (26)$$

This system can be regarded as a special case of the Appell-Hamel problem [4,5]. Trajectory snippets of motorsleds operated in reverse,  $p < 0$ , are displayed in Fig. 5. For a positive force,  $p > 0$ , the sled performs with relatively smooth random motion with little or no tumbling because the propulsion force accelerates the sled in its stable direction. For negative self-propulsion forces,  $p < 0$ , the sled is driven into its unstable direction, and the result is more frequent tumbling.

##### A. Stability analysis

The stability of the Eqs. (26) in the noiseless regime  $\xi_v(t) = \xi_\omega(t) = 0$  is analyzed in Fig. 6. On imposing  $\dot{v} = 0$  in the

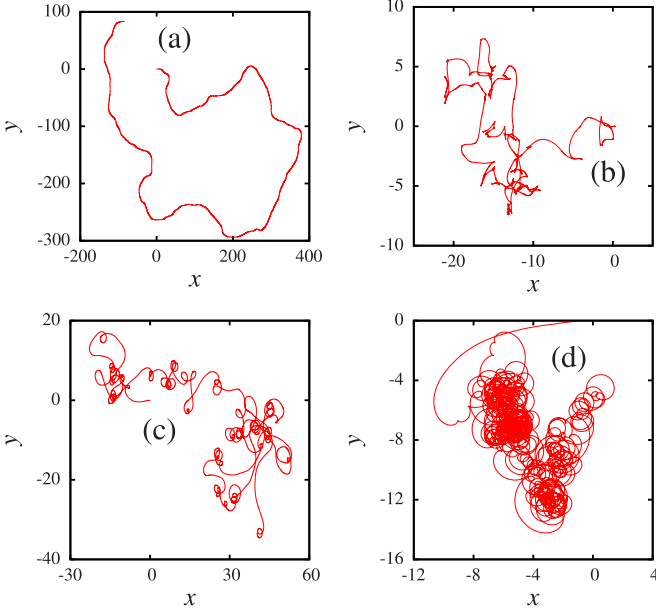


FIG. 5. Trajectory snippets of a stochastic motorsled with  $\alpha = 0.5$ ,  $\theta = 0.5$ ,  $\gamma = 1$ , and (a)  $p = 5.0$ , (b)  $p = -0.1$ , (c)  $p = -4.0$ , and (d)  $p = -15$ . These values of  $p$  correspond to the different diffusive regimes of Fig. 8. All snippets have the same time duration, whereas their spatial axes have been scaled to fit the frame size.

first equation we obtain the identity  $v = (p + \alpha\omega^2)/\gamma$ , which inserted in the second equation yields

$$\dot{\omega} = -\omega\Gamma\left[\left(1 + \frac{p}{|p_t|}\right) + \frac{\alpha}{|p_t|}\omega^2\right] \equiv -\frac{d}{d\omega}U(\omega), \quad (27)$$

where

$$p_t = -\gamma\Gamma(1 + \alpha^2)/\alpha < 0 \quad (28)$$

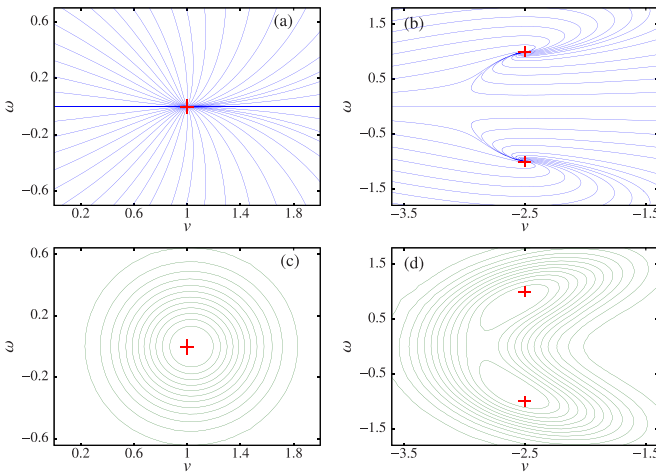


FIG. 6. Stability analysis of the stochastic motorsled model with  $\alpha = 0.5$ ,  $\Gamma = \gamma = 1$ , and  $p = 1$  [panels (a) and (c)] and  $p = -3$  [panels (b) and (d)]. Panels (a) and (b): Noiseless trajectories. Panels (c) and (d): Contour plots of the probability densities  $P(v, \omega)$  for  $\theta = 0.1$ . Crosses represent the stable points:  $\Phi_0$ , panels (a) and (c), and  $\Phi_{\pm}$ , panels (b) and (d).

and  $U(\omega)$  is an effective quartic potential.  $U(\omega)$  is monostable, with a minimum at  $\omega_0 = 0$ , for  $p \geq p_t$  (stable motorsled), and bistable, with minima at

$$\omega_{\pm} = \pm\sqrt{(p_t - p)/\alpha}, \quad (29)$$

for  $p < p_t < 0$  (unstable motorsled). Accordingly, the noiseless dynamics of Eq. (26) gives one fixed point in the momentum space  $v, \omega$  for  $p > p_t$ ,  $\Phi_0 = (v_0, 0)$  with  $v_0 = p/\gamma$ , and two fixed points for  $p < p_t$ ,  $\Phi_{\pm} = (v_t, \omega_{\pm})$  with  $v_t = p_t/\gamma$  [Fig. 6(a)]. An unstable motorsled thus performs circular orbits with radius  $r_t$ , where

$$r_t^2 = \left(\frac{v_t}{\omega_{\pm}}\right)^2 = (1 + \alpha^2)\frac{\Gamma}{\gamma}\frac{|p_t|}{p_t - p},$$

which shrinks as  $p$  grows smaller than  $p_t$  [Fig. 6(b)]. The transition of  $U(\omega)$  from a monostable to a bistable potential by lowering  $p$  across the critical value  $p_t$  amounts to a spontaneous breaking of the  $\omega \rightarrow -\omega$  symmetry of Eqs. (26).

This point is further illustrated by linearizing Eqs. (26) around their fixed points, namely,

$$\delta\dot{v} = -\gamma\delta v, \quad (30)$$

$$\delta\dot{\omega} = -\Gamma(1 + p/|p_t|)\delta\omega,$$

around  $\Phi_0$ , and

$$\delta\dot{v} = -\gamma\delta v + 2\alpha\omega_{\pm}\delta\omega, \quad (31)$$

$$\delta\dot{\omega} = -[\alpha/(1 + \alpha^2)]\omega_{\pm}\delta v,$$

around  $\Phi_{\pm}$ . [The dynamics around  $\Phi_{-}$  is symmetric under replacing  $\omega_{\pm} \rightarrow -\omega_{\pm}$ .] In both cases  $\delta v$  and  $\delta\omega$  denote the displacement of  $v$  and  $\omega$  with respect to the respective fixed values. One notices by inspection that all three fixed points are attracting with  $\Phi_0$  a sink node [the trajectories converge toward  $\Phi_0$  from all directions] and  $\Phi_{\pm}$  spiral sinks with opposite chirality [the trajectories approach  $\Phi_{\pm}$  spiraling, respectively, clockwise and counterclockwise, Fig. 6(b)]. The spiraling dynamics around  $\Phi_{\pm}$  can be better visualized by taking the time derivative of the corresponding linearized equations, that is,

$$\delta\ddot{v} = -\gamma\delta\dot{v} - \Omega^2\delta v, \quad \delta\ddot{\omega} = -\gamma\delta\dot{\omega} - \Omega^2\delta\omega, \quad (32)$$

with  $\Omega^2 = 2\omega_{\pm}^2\alpha^2/(1 + \alpha^2)$ . In this formalism, the trajectory orientation around  $\Phi_{\pm}$  has to be set as an appropriate initial condition.

We remark that the present stability analysis for the self-propelled CC sled differs from that found in the current literature on nonholonomic dynamics [7], due to the presence of the viscous terms  $-\gamma v$  and  $-\Gamma\omega$ . With regard to this, we notice that as  $\gamma$  and  $\Gamma$  tend to zero,  $p_t$  vanishes, so that, as expected, for  $p < 0$  there are two symmetric fixed points,  $\Phi_{\pm} = (\pm|p|, 0)$ , and for  $p > 0$  none ( $\Phi_0$  moves up to infinity) [8]. In the frictionless regime,  $\Phi_{\pm}$  are center fixed points, around which the trajectories trace (clockwise and counterclockwise) closed orbits of the equation  $v^2 = v_M^2 - (1 + \alpha^2)(\alpha\omega^2 - |p|)/\alpha + |p|\ln(\alpha\omega^2/|p|)$ , for any  $v_M \neq 0$ .

## B. Velocity moments

The additive noises  $\xi_v(t)$  and  $\xi_{\omega}(t)$  do not change the stability properties of the linearized Langevin Eqs. (30) and

(31). This is confirmed by the contour plots of Fig. 6, which show how the probability densities  $P(v, \omega)$ , obtained by numerical simulation, peak in the vicinity of  $\Phi_0$  for  $p > p_t$ , panel (c), and  $\Phi_{\pm}$  for  $p < p_t$ , panel (d). The shift of the  $P(v, \omega)$  peaks from the fixed points  $\Phi_0$  and  $\Phi_{\pm}$  is due to the absence of a detailed balance in Eqs. (8) and, therefore, Eq. (26), for  $\alpha \neq 0$ .

The first moment of the observable  $v(t)$  as a function of  $p$  can be calculated as follows. The expression of Eq. (12) for  $\langle v \rangle$  is now modified to account for the force  $p$ ,  $\langle v \rangle = (p + \alpha \langle \omega^2 \rangle) / \gamma$ . At low temperatures, the quantity  $\langle \omega^2 \rangle$  can be estimated from the linearized Langevin Eqs. (30) and (31) upon restoring the noise terms of Eqs. (26), namely,

$$\begin{aligned} \delta \dot{v} &= -\gamma \delta v + \sqrt{\gamma \theta} \xi_v(t), \\ \delta \dot{\omega} &= -\Gamma \left( 1 - \frac{p}{p_t} \right) \delta \omega + \sqrt{\frac{\Gamma \theta}{1 + \alpha^2}} \xi_{\omega}(t), \end{aligned} \quad (33)$$

for  $p > p_t$ , and

$$\begin{aligned} \delta \dot{v} &= -\gamma \delta v + 2\alpha \omega_{\pm} \delta \omega + \sqrt{\gamma \theta} \xi_v(t), \\ \delta \dot{\omega} &= -\frac{\alpha}{1 + \alpha^2} \omega_{\pm} \delta v + \sqrt{\frac{\Gamma \theta}{1 + \alpha^2}} \xi_{\omega}(t), \end{aligned} \quad (34)$$

in the neighborhood of  $\omega = \omega_{\pm}$  for  $p < p_t$ . A simple moment analysis [14] yields  $\langle \delta v \rangle = \langle \delta \omega \rangle = 0$  and

$$\langle \delta v \delta \omega \rangle = 0, \quad \langle \delta v^2 \rangle = \theta, \quad \langle \delta \omega^2 \rangle = \frac{\theta}{1 + \alpha^2} \frac{|p_t|}{p - p_t}, \quad (35)$$

for  $p \gg p_t$ , and

$$\begin{aligned} \langle \delta v \delta \omega \rangle &= \frac{\Gamma \theta}{\alpha \omega_{\pm}}, \quad \langle \delta v^2 \rangle = \theta \left( 1 + 2 \frac{\Gamma}{\gamma} \right), \\ \langle \delta \omega^2 \rangle &= \frac{\theta}{2(1 + \alpha^2)} \left( 1 + 2 \frac{\Gamma}{\gamma} \right) + \frac{\theta \gamma \Gamma}{2\alpha^2 \omega_{\pm}^2}, \end{aligned} \quad (36)$$

for  $p \ll p_t$ . Accordingly, the approximated expressions for  $\langle v \rangle$  are

$$\langle v(p) \rangle = p/\gamma + \theta \Gamma / (p - p_t), \quad (37)$$

for  $p \gg p_t$ , and

$$\langle v(p) \rangle = \frac{p_t}{\gamma} + \frac{\theta}{2\gamma} \frac{\alpha}{1 + \alpha^2} \left( 1 + 2 \frac{\Gamma}{\gamma} \right) + \frac{\theta \Gamma}{2(p_t - p)}, \quad (38)$$

for  $p \ll p_t$ . Predictions in Eqs. (37) and (38) compare well with the numerical data reported in Fig. 7.

In conclusion, for appropriately low  $\theta$  values, the curves  $\langle v(p) \rangle$  approach the oblique asymptote  $\langle v_{+} \rangle = p/\gamma$  for  $p \rightarrow +\infty$  and the horizontal asymptote  $\bar{v}_{-} = -|p_t|/\gamma$  for  $p \rightarrow -\infty$ , with a zero at  $p_0 = -\alpha \langle \omega^2(\epsilon) \rangle \simeq -\alpha \theta / (1 + \alpha^2)$  (stopping force). We remark that, in the regime of validity of the present analysis,  $p_0$  and  $p_t$  satisfy the inequality  $p_t < p_0$  and tend to the same limits, respectively,  $p_0 = 0$  and  $p_t = -\infty$ , for both  $\alpha \rightarrow 0$  and  $\alpha \rightarrow \infty$ . From a physical viewpoint this means that propelling the sled in the stable direction boosts its mobility, whereas propelling it in the opposite direction increases the tumble rate and thus suppresses  $\langle v(p) \rangle$ . Suppression by tumbling is more prominent around  $\alpha = 1$ , where  $|p_t|$  has a minimum.

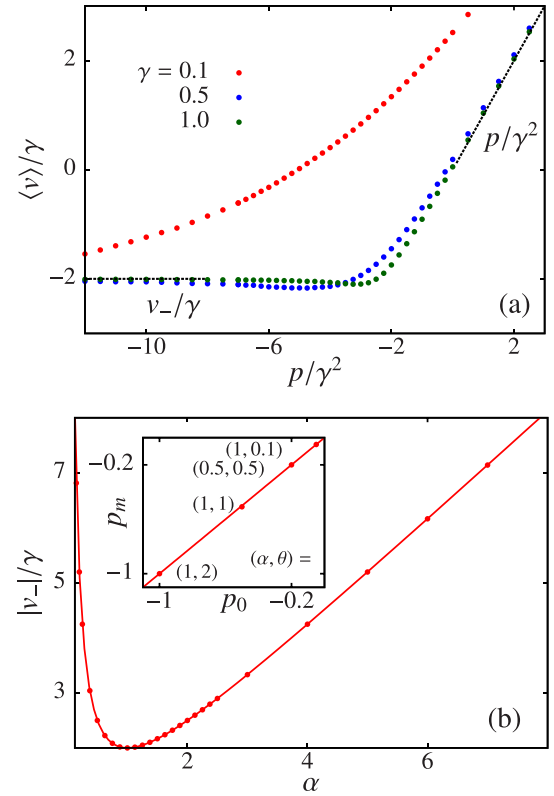


FIG. 7. Dynamical instability of a propelled sled. (a)  $\langle v \rangle$  vs  $p$  for  $\alpha = 1$ ,  $\theta = 0.1$ , and different  $\gamma$  (see legends). Numerical data points approach the predicted asymptotes  $\bar{v}$  for  $p \rightarrow \pm\infty$  [Eqs. (37) and (38), dashed lines]. (b)  $|v_{-}|$  vs  $\alpha$  for  $\gamma = 1$ ; simulation data points are plotted against the analytical curve of Eq. (38). Inset: The corresponding stopping force: the numerical estimate,  $p_m$ , vs the analytical prediction,  $p_0$ .

The  $p$  dependence of the kinetic energy follows immediately from the approximate expressions for  $\langle v(p) \rangle$  in Eqs. (37) and (38). We compare here the asymptotic behaviors of the translational energy  $\langle E_v \rangle = (1/2) \langle v^2 \rangle$  and the rotational energy  $\langle E_{\omega} \rangle = (1/2)(1 + \alpha^2) \langle \omega^2 \rangle$ , by singling out the leading terms in  $|p|$  for  $|p/p_t| \gg 1$ . For  $p \gg p_t$ ,  $\langle \omega^2 \rangle = \langle \delta \omega^2 \rangle \simeq \theta(\gamma \Gamma / \alpha p)$  is negligible; hence

$$\langle E \rangle \simeq \langle E_v \rangle = p^2 / 2\gamma^2.$$

Vice versa, for  $p \ll p_t$  the translational term of the kinetic energy approaches a constant,  $\langle E_v \rangle \simeq v_-^2 / 2 = |p_t|^2 / 2\gamma^2$ , while the rotational term increases with  $|p|$ ,  $\langle E_{\omega} \rangle \simeq (1 + \alpha^2) \omega_{\pm}^2 / 2 = p_t(p - p_t) / (2\gamma \Gamma)$ . By adding these two quantities we obtain

$$\langle E \rangle = (p_t / 2\gamma) [p / \Gamma - p_t(\Gamma^{-1} - \gamma^{-1})] \simeq pp_t / (2\gamma \Gamma).$$

This result corroborates the mechanisms of mobility suppression by dynamical instability. The total kinetic energy  $\langle E \rangle$  grows quadratically with  $p$  in the limit  $p \rightarrow +\infty$  and linearly only in the opposite limit  $p \rightarrow -\infty$ . Indeed, pushing the sled harder in the stable direction increases its translational energy, while pushing it in the unstable direction only makes it rotate faster.

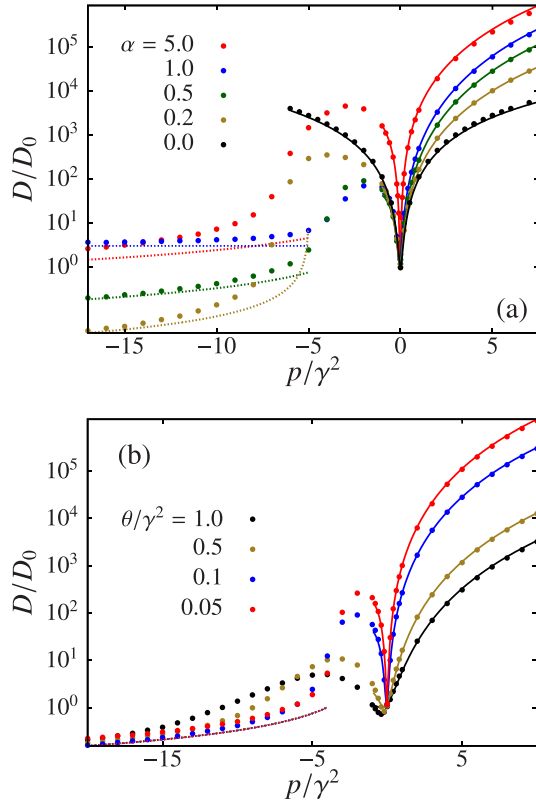


FIG. 8. Dynamical instability of a propelled sled:  $D$  vs  $p$  for  $\gamma = 1$ . (a)  $\theta = 0.5$  and different  $\alpha$ . (b)  $\alpha = 0.5$  and different  $\theta$  (see legends). Data (points) from numerical integration and approximate curves for  $D(p)$  [Eqs. (39), solid lines, and (42), dashed lines] are compared.

### C. Diffusion

We conclude this section by calculating the diffusion coefficient  $D$  as a function of the self-propulsion force  $p$  at low temperature. We do so by applying again Kubo's formula, Eq. (18), to the linearized version of the motorsled's Langevin equations, Eqs. (30) for  $p > p_t$  and Eqs. (31) for  $p < p_t$ .

For  $p > p_t$  and  $\epsilon \ll 1$  the derivation of  $D$  follows step by step the derivation of Eq. (22), except that  $D_\phi$  is now replaced by  $D_\phi \rightarrow D_\phi/(1 + p/|p_t|)^2$  [see second Eq. (33)] and  $\langle v(\alpha) \rangle$  by  $\langle v(p) \rangle$ , Eq. (37), to account for the force  $p$ . With this substitution, the first equality in Eq. (22) still applies, whereas the second equality, correct in leading order of  $\epsilon$ , now reads

$$D(p) \simeq \frac{\theta}{2\gamma} \left[ 1 + \frac{\Gamma}{\gamma} \frac{\alpha^2}{1 + \alpha^2} \left( 1 + \frac{p(p - p_t)}{p_t p_0} \right)^2 \right], \quad (39)$$

with  $p_0$  as defined in Sect. IV B. For  $\alpha = 0$  and large  $p$  the approximate expression of Eq. (39) coincides with the outcome of an exact calculation [16],  $D(p) = (p/\gamma)^2 \Gamma/2\theta$  [see Fig. 8(a)]. However, a crossover from a quadratic to a quartic power law is predicted in the interval  $|p_0| < p < |p_t|$ , for  $\alpha > 0$ . The above estimate for  $D(p)$  appears to be in close agreement with the numerical data of Fig. 8 even for values of  $p$  well to the left of the minimum of  $D(p)$ ,  $p_m \simeq p_0$ , which corresponds with the zero of  $\langle v(p) \rangle$ . The coincidence of the

minimum of  $D(p)$  with the zero of  $\langle v(p) \rangle$  is illustrated in the inset of Fig. 7(b).

For  $p \ll p_t$ , the autocorrelation function to be inserted in Kubo's formula, Eq. (18), factorizes as

$$\begin{aligned} C(t) &= v_-^2 \langle \cos \phi(t) \cos \phi(0) \rangle \\ &\quad + \langle \delta v(t) \delta v(0) \cos \phi(t) \cos \phi(0) \rangle \\ &\simeq \cos(\omega_\pm t) \langle \cos \delta \phi(t) \cos \delta \phi(0) \rangle [v_-^2 + \langle \delta v(t) \delta v(0) \rangle], \end{aligned} \quad (40)$$

where  $\delta \phi(t) = \phi(t) - \omega_\pm t$ ,  $v_-$  is the leading term of Eq. (38),  $v_- = -|p_t|/\gamma$ , and we made use of the linearization arguments of Sec. IV A to set the cross terms  $\langle \sin \delta \phi(t) \cos \delta \phi(0) \rangle$  to zero. From the linearized Langevin equations of the preceding section, we also have

$$\langle \delta v(t) \delta v(0) \rangle = \langle \delta v^2 \rangle e^{-\gamma t/2} \cos(\omega_1 t), \quad (41)$$

with  $\langle \delta v^2 \rangle = (1 + 2\Gamma/\gamma)\theta$  and  $\omega_1^2 = \Omega^2 - (\gamma/2)^2$ . The angular fluctuations,  $\cos \delta \phi(t)$ , decay much slower than the speed fluctuations,  $\delta v(t)$ , namely,  $\langle \cos \delta \phi(t) \cos \delta \phi(0) \rangle = (1/2)e^{-\tilde{D}_\phi t}$ , with  $\tilde{D}_\phi = (D_\phi/4)[p_t/(p_t - p)]^2$ . The effective diffusion constant  $\tilde{D}_\phi$  has been extracted from the linearized Langevin equation,

$$\dot{\omega} = -dU(\omega)/d\omega - \Gamma\omega + \sqrt{\Gamma\theta/(1 + \alpha^2)} \xi_\omega(t)$$

[see Eq. (27)], upon expanding  $U(\omega)$  in the neighborhood of its minima  $\pm\omega_\pm$ . As a consequence, the spatial diffusion of an unstable motorsled is governed by the fluctuations of its longitudinal velocity,  $v(t)$ . Accordingly, to compute Kubo's integral in leading order it suffices to approximate  $C(t) \simeq (1/2)\langle \delta v(t) \delta v(0) \rangle \cos(\omega_\pm t)$ ; hence

$$D(p) \simeq \frac{\theta}{4\gamma} \frac{(1 + 2\Gamma/\gamma)(\gamma/\omega_\pm)^2 [1 + 2\alpha^2/(1 + \alpha^2)]}{[1 - 2\alpha^2/(1 + \alpha^2)]^2 + (\gamma/\omega_\pm)^2}. \quad (42)$$

This asymptotic expression for  $D(p)$  is inverse proportional to  $\omega_\pm^2$ ; the sled's diffusivity is thus suppressed according to the power law

$$\frac{D(p)}{D_0} \propto \frac{p_t}{p_t - p}, \quad (43)$$

for all  $\alpha$  except for  $\alpha = 1$ , where  $D(p) = (1 + 2\Gamma/\gamma)D_0$ . The estimates of Eqs. (39) and (42) for  $D(p)$  are in close agreement with the simulation results plotted in Fig. 8(b), where for  $p > p_t$  and  $p \ll p_t$  the ratio  $D(p)/D_0$  is apparently independent of  $\theta/\gamma^2$ . The case  $\alpha = 1$  is remarkable. The horizontal asymptote of  $D(p)$  for  $p \rightarrow -\infty$  signals a sort of *resonant diffusion* effect: For  $\alpha = 1$  the angular frequency associated with the symmetry breaking mechanism,  $\omega_\pm$ , and the angular frequency of the orbits spiraling around the fixed points  $\Phi_\pm$  in the  $v, \omega$  plane,  $\Omega$ , coincide; as a consequence, the sled diffuses insensitive to  $p$ , as if it were a *free* Brownian particle with the effective temperature  $(1 + 2\Gamma/\gamma)\theta/4$ .

The existence and position of the  $D(p)$  peak are consistent with the phenomenological analysis of Ref. [17], according to which the dependence of the drift speed,  $\langle v \rangle$ , and the diffusivity curve,  $D$ , on the external driving parameter,  $p$ , would be closely related. In particular, an excess diffusion peak is expected to occur where the gradient of  $|\langle v \rangle|$  has a maximum,

that is, for  $p \sim p_t$ . A comparison of the numerical data of Figs. 7(a) and 8(a) for  $p < p_0$  confirms such a coincidence.

## V. CONCLUSIONS

As an additional motivation of the present work, we point out similarities of the behavior of our stochastic nano-motorsled and the tumble-and-run dynamics of active microswimmers at low Reynolds numbers. An artificial microswimmer enhances its diffusivity by harvesting kinetic energy from an active suspension fluid [10,11], as a result of some sort of functional asymmetry of its own [18,19]. The active particle thus propels itself with constant speed  $v_0$ , as if subjected to an effective propulsion force [20],  $p$ , such that  $v_0 = p/\gamma$ . However, its center of mass and the center of the effective force propelling it (say, a bimetallic colloidal Janus particle [10]) may well not coincide. The nano-motorsled can then stylize a wide class of eccentric artificial microswimmers.

As an experimental example, we mention the reported case [21] of an active swimmer moving in a thin layer of suspension fluid, subject to gravity: If the substrate is touched with a snag, this acts as a pivot point, very much like the blade of a sled. For a noneccentric swimmer,  $\alpha = 0$ , the approximate expression derived for the diffusion constant, Eq. (39), in the limit of large  $p$ , coincides with the quadratic expression adopted in the current literature,  $D = v_0^2/2D_\phi$ , as long as one identifies  $v_0 = p/\gamma$  and  $D_\phi = \theta/\Gamma$ .

Vice versa, for  $\alpha > 0$  a motorsled operated in the unstable mode behaves like an overdamped microswimmer with propulsion speed  $v_0$  and angular frequency  $\pm\omega_1$  [see Eq. (41)]. It will spiral either clockwise or counterclockwise [22], switching orientation at random. The ensuing random sequence of runs and tumbles is thus predicted to suppress the swimmer's diffusivity, no matter how strong the applied force (e.g., the fuel concentration in the suspension [19]).

- 
- [1] S. A. Chaplygin, *Mat. Sbornik* **28**, 303 (1911) (in Russian).
  - [2] C. Carathéodory, *Z. Angew. Math. Mech.* **13**, 71 (1933) (in German).
  - [3] See for a review A. M. Bloch, *Nonholonomic Mechanics and Control* (Springer, New York, 2003).
  - [4] P. Appell, *Rend. Circ. Mat. di Palermo* **32**, 48 (1911) (in French).
  - [5] G. Hamel, *Theoretische Mechanik* (Springer, Berlin, 1967), Chap. 9 (in German).
  - [6] N. A. Fufaev, *Prikl. Math. Mech.* **28**, 513 (1964) [*J. Appl. Math. Mech.* **28**, 630 (1964)].
  - [7] For a review see Ju. I. Neimark and N. A. Fufaev, *Dynamics of Nonholonomic Systems*, Translations of Mathematical Monographs Vol 33 (American Mathematical Society, Providence, 2004).
  - [8] V. M. Budanov and Ye. A. Devyanin, *J. Appl. Maths Mechs.* **67**, 215 (2003).
  - [9] M. J. McBride, *Annu. Rev. Microbiol.* **55**, 49 (2001); H. C. Berg, *E. Coli in Motion* (Springer, New York, 2013).
  - [10] S. Jiang and S. Granick (Editors), *Janus Particle Synthesis, Self-Assembly and Applications* (RSC Publishing, Cambridge, UK, 2012); A. Walther and A. H. E. Müller, *Chem. Rev.* **113**(7), 5515 (2013).
  - [11] F. Schweitzer, *Brownian Agents and Active Particles* (Springer, Berlin, 2003); S. Ramaswamy, *Annu. Rev. Condens. Matter Phys.* **1**, 323 (2010).
  - [12] A. Budo, *Theoretische Mechanik* (Verlag der Deutschen Wissenschaften, Berlin, 1976).
  - [13] C. W. Gardiner, *Handbook of Stochastic Methods* (Springer, Berlin, 1985).
  - [14] H. Risken, *The Fokker-Planck Equation* (Springer, Berlin, 1986).
  - [15] Y. Li, P. K. Ghosh, F. Marchesoni, and B. Li, *Phys. Rev. E* **90**, 062301 (2014); X. Ao, P. K. Ghosh, Y. Li, G. Schmid, P. Hänggi, and F. Marchesoni, *Eur. Phys. J.: Spec. Top.* **223**, 3227 (2014).
  - [16] A. Nourhani, V. H. Crespi, and P. E. Lammert, *Phys. Rev. E* **90**, 062304 (2014).
  - [17] G. Costantini and F. Marchesoni, *Europhys. Lett.* **48**, 491 (1999).
  - [18] R. Golestanian, T. B. Liverpool, and A. Adjari, *New J. Phys.* **9**, 126 (2007).
  - [19] See, e.g., Y. Hong, D. Velegol, N. Chaturvedi, and A. Sen, *Phys. Chem. Chem. Phys.* **12**, 1423 (2010).
  - [20] B. ten Hagen, R. Wittkowski, D. Takagi, F. Kümmel, C. Bechinger, and H. Löwen, *J. Phys.: Condens. Matter* **27**, 194110 (2015).
  - [21] D. Takagi, A. B. Braunschweig, J. Zhang, and M. J. Shelley, *Phys. Rev. Lett.* **110**, 038301 (2013).
  - [22] S. van Teeffelen and H. Löwen, *Phys. Rev. E* **78**, 020101 (2008).